

GT2011-45888

## NUMERICAL AND EXPERIMENTAL INVESTIGATIONS OF A COMPRESSOR CASCADE FLOW WITH SECONDARY AIR REMOVAL

Sascha Pönick\*, Dragan Kožulović, Rolf Radespiel  
Institut für Strömungsmechanik  
Technische Universität Braunschweig  
Bienroder Weg 3, 38106 Braunschweig, Germany  
Email: s.poenick@tu-bs.de

Bernd Becker, Volker Gümmer  
Rolls-Royce Deutschland Ltd. & Co. KG  
Eschenweg 11, Dahlewitz,  
15827 Blankenfelde-Mahlow, Germany  
Email: bernd.becker@rolls-royce.com

### ABSTRACT

The paper presents numerical and experimental results for a low speed compressor cascade with bleed air removal at the endwall. The aerofoil design is representative for a stator blade in a modern high pressure compressor near the casing wall. Secondary air is commonly supplied by simple bleed geometries downstream of stator rows. The focus of the present investigation was the systematic development of a passage integrated bleed configuration which, with the constraint of an invariable bleed mass flow rate, provides advantageous effect on the main flow and furthermore a high pressure recovery in the bleed flow. Steady 3D RANS simulations were performed using the Spalart-Allmaras turbulence model. In both, numerical simulations and experiments, an improved performance was found. Beside reduced losses and increased pressure rise the wake flow downstream of the customized bleed geometry was found to be more homogeneous with decreased deviations due to a favorable influence on the secondary flow.

### NOMENCLATURE

#### Geometric and Flow quantities

$\alpha, \beta, i$	Flow angles
$\lambda$	Stagger angle
$\mu$	Axial velocity ratio
$\zeta_V$	Loss coefficient ( $\zeta_V = (p_{t1} - p_{t2})/q_1$ )
$c_p$	Pressure coefficient ( $c_p = (p_{x,y,z} - p_1)/q_1$ )
$\Delta p/q$	Pressure recovery

$D$	Diffusion Number
$\delta$	Boundary layer thickness
$H$	Blade height
$l$	Chord length
$m'$	Streamwise coordinate
$t$	Pitch
$p$	Static pressure
$p_t$	Stagnation pressure
$q$	Dynamic head
$s$	Radial gap width
$x, y, z$	Cascade coordinate system

#### Indices

1	Inlet plane (1/3 upstream LE)
2	Measuring plane (1/3 downstream TE)
Bleed	Bleed (analysis plane)
Ref	Reference

#### Abbreviations

RANS	Reynolds-averaged Navier-Stokes
CDA	Controlled Diffusion Airfoil
NACA	National Advisory Committee for Aeronautics
VBP	Vortex Bleed Port
SS	Suction side
PS	Pressure side
TE	Trailing edge
LE	Leading edge

\*Address all correspondence to this author.

## INTRODUCTION

The compression system has significant influence on weight and efficiency of an aero-engine or gas turbine. Within the last decade successive improvements in compressor aerodynamics were accomplished. Especially high-capacity CFD tools allowed to simulate and analyze complex flow phenomena within research and the design process, *Cumpsty* [1].

Despite of all evolution, one of the inevitable loss sources is the secondary air system of the gas generator. Commonly, the bleed air decreases the overall efficiency depending on the removed massflow rate and the pressure level accordingly the stage number where it is removed from the core flow. In operational engines the secondary air use reaches up to 30 percent of the core massflow due to additional air demand for cabin climate control and deicing. Recent engine-concepts also need a secondary air system which at least supplies high pressure fluid for turbine cooling purposes. Beside proceeding improvements in cooling effectiveness and concepts like cooled cooling air which promise a further reduction of bleed air consumption, one important issue is to advance the secondary air removal in the compressor stage. Commonly for the customer bleed a high pressure recovery of the bleed massflow and minimum interference to the main gas path besides structural requirements are aspired.

In literature, much research work about the bleed air distribution system downstream of the actual bleed port is published. *Bowman, Gomes and Schwarz* [2] - [4] investigated principle loss-mechanism in a secondary air system with the aim to improve existing correlations by means of CFD simulations and experiments of secondary components such as annulus plenum and connecting pieces. Further work has been done about experimental and numerical calibration of flow losses of bleed via slot and hole arrays as they are commonly used for boundary layer removal, *Willis* [5].

*Leishman et al.* [6] - [8] accomplished comprehensive studies about secondary air bleed in stator cascades. In [6] both experimental and numerical results for variable bleed through circular holes within the passage were introduced. They proved that the pressure recovery highly depends on the position within the passage. Secondary effects within the bleed cavity disturb the primary flow especially for low bleed rates. The investigated geometries were customized and added by ramp and slot geometries to influence the secondary flow and loss behavior, [7] and [8]. Here, the bleed configurations, which were dimensioned for a broad massflow range up to ten percent with accordingly large sectional areas, were afflicted with strong secondary flow phenomena for low and medium bleed fractions, too.

*Gümmer* [9] used a bleed port configuration which will be used as reference for present performance evaluation. This tailored bleed port is characterized by an effective removal of a developed corner separation on the blade suction side adjacent to the endwall. In Fig. 1 an overview of prescribed bleed port designs and positions within the compressor passage is given.

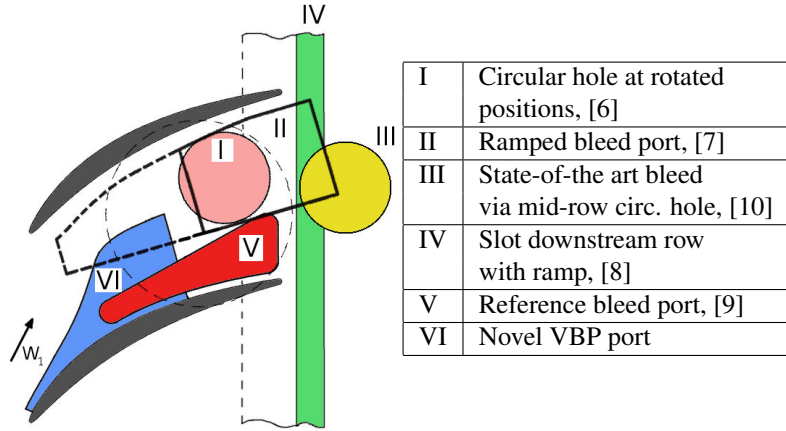


FIGURE 1. Bleed port designs and positions

## DESIGN APPROACH

The design intention of the present work was to develop a bleed port configuration which primarily has positive influence on the main flow in terms of loss coefficient and pressure rise. Secondary a high pressure recovery of the bleed air was requested. This should be accomplished by the definition of a constant design bleed rate of three percent referred to the actual passage flow amount. Moreover, preliminary numerical investigations of bleed via sloped circular holes indicated an advantage of an early extraction near the suction side surface. By means of a continuous removal of the skewed endwall boundary layer starting in the front section on the blade the development of the typical cross passage flow can be essentially weakened. However, by positioning a bleed cavity that near to the suction peak the strong pressure gradients amplify secondary flow phenomena within the cavity itself. In other words, one general trend

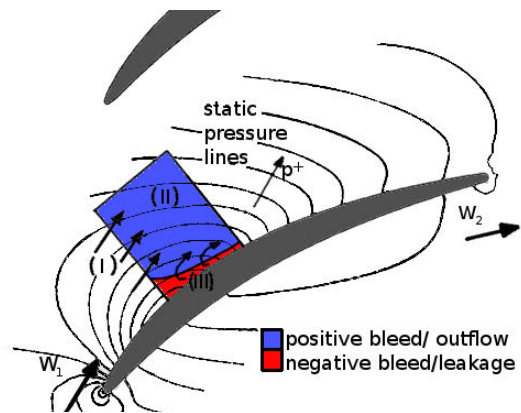


FIGURE 2. Problem of negative bleed for passage integrated bleed offtake

of the bleed air is to maintain its flow direction (marked (I) in Fig. 2) and concentrate the removal in the area (II) toward the pressure side of the neighboring blade. Thereby a high risk of low momentum flow leakage back into the passage in fields of low pressure near the suction side surface (III) has to be beard. The flow performance of the main passage is degenerated very strongly by that negative bleed effect. Interestingly, this unfavorable effect for the core flow becomes even worse if one tries to adapt the bleed geometry to the bleed flow by means of ramps and radii. Nevertheless, the stagnation pressure loss and hence the pressure recovery of the bleed air is continuously improved by that.

A new approach was to take advantage of the principle of a sub-merged NACA inlet, Frick [11]. Thereby a vortex pair discharges fluid into the cavity leading to a high flow rate and pressure recovery with low interference with the overlying main flow. A geometry configuration with a curved sidewall and ramp contour was designed according to required space limits in the cascade. The bleed port was positioned to the local flow direction providing a continuous vortex formation by the sweep back shape of the duct sidewall (See Fig. 9). Continued numerical investigations evolved to a single-edge contoured bleed port geometry adjacent to the blade suction side which will be presented as the *VBP* (longitudinal vortex bleed port) in this paper.

### NUMERICAL PROCEDURE

The 3D RANS simulations presented in this paper were performed with NUMECAs FINE/Turbo<sup>TM</sup> [12]. Therefore the cascade was discretized by a multi-block (H-O-H topology) mesh with approximately 3.6 million structured cells. For taking advantage of the multigrid method meshes with at least three grid levels have been generated. The inlet and outlet boundaries were situated one and a half chord length up- and downstream of the blade respectively. Early simulations indicated that the fluid removal at only one of the endwalls causes severe three-dimensional effects in the low aspect ratio cascade. The occurrence of a complete corner stall at the opposing endwall for well performing bleed configurations did not promise a practicable flow evaluation. In contrast to a symmetric setup with air removal on both endwalls a one-sided offtake meets the conditions in the machine hence the redistribution effects are also from interest. Finally a radial gap was appended at the opposite endwall forming a tip leakage vortex which reacts less sensitive to flow changes like axial velocity and incidence.

The bleedport cavities were meshed with up to 1.6 million additional hexahedrals and linked to the main passage via non-matching connections. This approach provided by the solver environment allowed the investigations of different bleed geometries in combination with constant meshing of the main gas path hence with accordingly low mesh sensitivity. For the non-matching connections comprehensive interpolation work has to

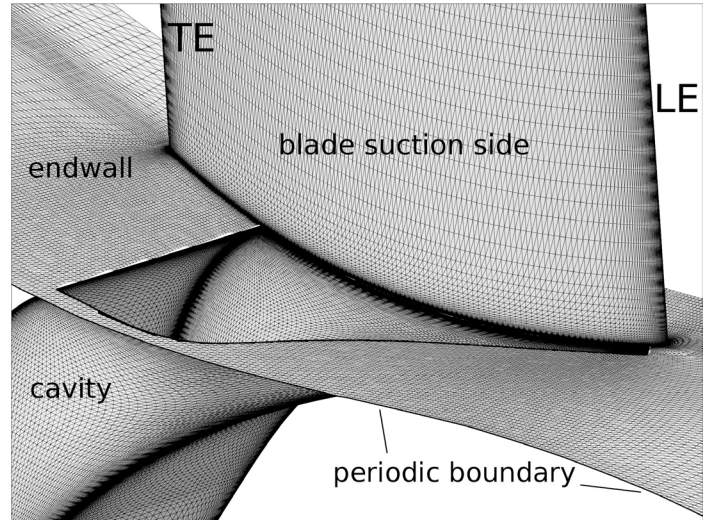


FIGURE 3. Mesh resolution in the bleed port environment

be done by the solver. To achieve good interpolation performance, special care has been taken to the mesh quality in that region, in particular with respect to cell expansion and width ratio. For the meshes a dimensionless wall distance value of  $y^+ \approx 5$  was aspired. In Fig. 3 the standard resolution mesh is shown. The solid boundaries at the VBP bleed port are visualized by means of an iso surface for computed wall distance zero. To assure the correct bleed flow ratio a fixed massflow boundary condition at the passage inlet and bleed port outlet was applied. Further, scaled spanwise velocity ratio distributions for the axial velocity  $V_x/V_1$  and the pitchwise velocity  $V_y/V_1$  which produce

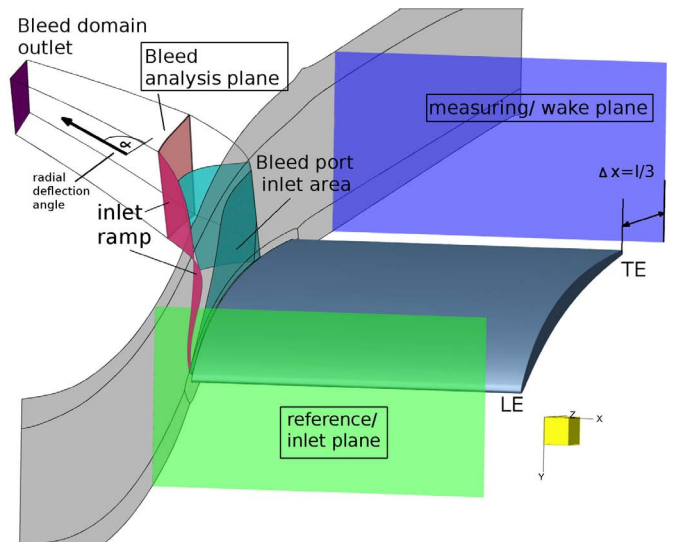


FIGURE 4. Integration planes for the CFD studies

the desired inlet angle  $\beta_1$  and a collateral boundary layer with the thickness  $\delta$  in the reference plane representative for the wind tunnel was prescribed. For an enhanced numerical stability of the bleed outlet an additional flow passage with decreased cross section was appended downstream of the real bleed port geometry.

For the presented steady simulations the Spalart-Allmaras turbulence model was applied. The spatial discretization used was a 2<sup>nd</sup> order upwind scheme for convective terms, and central differencing for diffusion terms. The code solves the RANS equations using an explicit time marching 4-step Runge-Kutta procedure. Convergence is accelerated by means of local time stepping, a full multigrid approach and implicit residual smoothing. The progress of the simulations was monitored by means of weighted and local density residuals. The computation work was performed parallelized with up to eight processors.

### Sensitivity of the numerical studies

To quantify the numerical uncertainties of the present flow phenomena numerous sensitivity studies have been accomplished. Simulations were performed regarding both, refined meshes up to 21 million cells respective half-sized cell width and a mesh topology avoiding the non-matching connections for a similar bleed configuration. Furthermore, other two-equation turbulence models were tested. The corresponding results indicate certain variations for the integral values. Up to 11 percent higher pressure recovery and lower loss coefficients for both the secondary air and the core flow were predicted by computations with further refined meshes. The simulations with full-matching connection between the bleed port and the passage generally showed an intensified vortex formation hence improving performance and stability. The variations due to turbulence modeling indicated slightly declined coefficients for the two-equation turbulence models. The observed flow phenomena and hence the trends in comparison of the bleed configurations remained almost unchanged. Despite the investigated variations the VBP bleed port remained superior to the reference persistently. Accompanying simulations with a modeled plenum box according to the experimental setup showed no influence on the calculated upstream cavity flow. Some of the sensitivity results are shown in the appendix of the paper.

### EXPERIMENTAL SETUP

The experiments were carried out in the low-speed cascade wind tunnel for low aspect ratios at the Institute of Fluid Mechanics of the Technische Universität Braunschweig. The test section has the dimensions of 200 mm x 500 mm and is shown in Fig. 5, [13]. An array of five CDA profiled vanes with fixed stagger angle and for the bleed configurations four secondary air removal ports at one of the endwalls was investigated. The

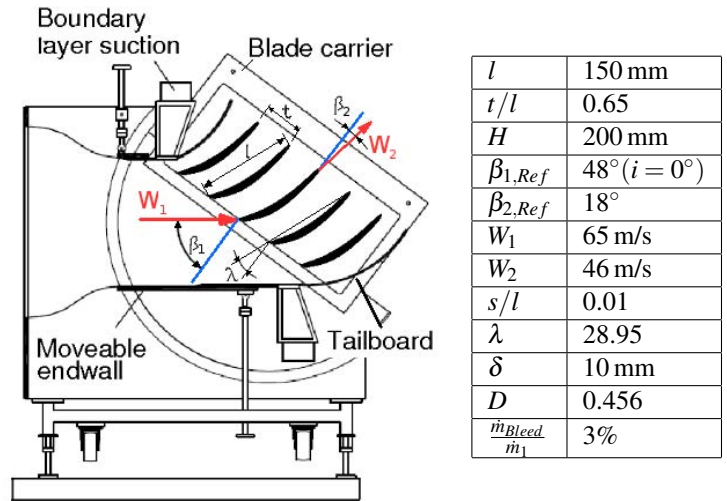


FIGURE 5. Test section of the cascade wind tunnel and geometry data

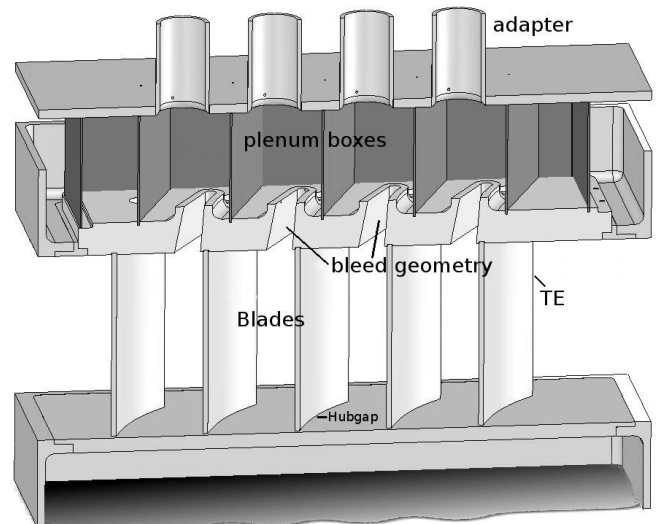
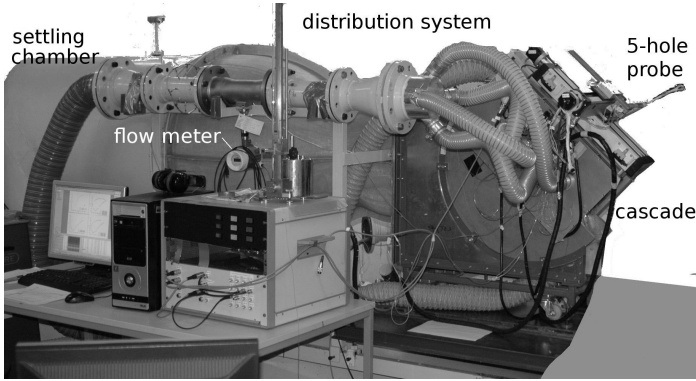


FIGURE 6. Cross sectional view of the reference bleed configuration installed

cascade geometry and wind tunnel data is summarized in the table within the figure. Periodic cascade flow was achieved by boundary layer suction at the tailboards and monitored by using the static pressure distribution in pitchwise direction in the inlet plane. The boundary layers on the vertical test section walls (endwalls) were not influenced. The boundary layer and the flow angles at the inlet plane were measured during preliminary investigations. The boundary layer thickness was found to be almost independent from the inlet angle and the maximum deviation between geometrically adjusted inlet angle and effective flow angle was  $\Delta\beta_1 \leq 0.2^\circ$ . The flow quantities were measured with a calibrated and 2D traversable mounted five-hole probe. The accuracy of the measured data within this paper is for the angles



**FIGURE 7.** Wind tunnel facility with pressure measurement equipment installed

$\pm 0.1\%$  and for the pressures coefficients  $\pm 1.5\%$ , [13].

A modular design was used for the bleed rig so that different bleed geometries could be investigated easily. In the assembly shown in Fig. 6 the blades were mounted at the same endwall as the bleed port forming an undisturbed hub gap at the opposite side required for flow stabilization. For the wind tunnel model fillet radii and overrunnings were avoided where possible to maintain the comparability to the numerical investigations of the simplified linear cascade geometry. The mass flow was determined by a volume meter in combination with temperature and pressure gauges and controlled by the rotational speed of the radial compressor in the secondary air system. The complete test setup is shown in Fig. 7. The pressure recovery of the bleed air flow was measured for each of the four treated passages by a pressure tap inside the corresponding plenum box. The achievement of periodic flow for a low aspect ratio cascade with non-symmetric fluid removal was found to be quite challenging so that conformity of test section had to be checked persistently by pressure traverse measurement and oil-flow visualization covering all passages.

The surface pressure measurements included eleven pressure taps within the VBP bleed port along the centerline of ramp and pressure taps at the midsection blade. Therefore a gauging blade was manufactured by stereolithography technique which enabled the simultaneous measurement of up to 135 pressure taps at the half-span facing the bleed port.

## RESULTS

The presentation of results will begin with the description of the flow phenomenology at both bleed configurations as it has been predicted by the CFD calculations. If not otherwise specified the results shown in the paper are for the aerodynamic design point at an inlet angle of  $\beta_{1,ref} = 48^\circ$  ( $i = 0^\circ$ ). In Fig. 8 a perspective view at the bleed ports and the corner between the blade suction side and the endwall is given. The core flow leads from

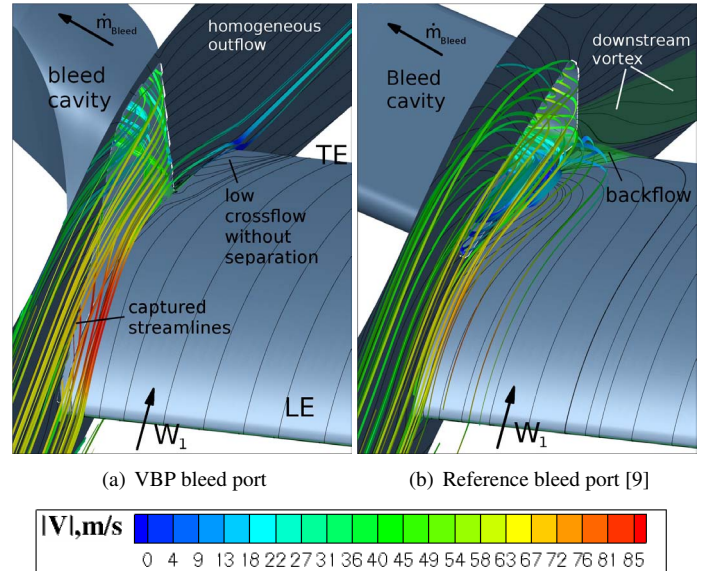


**FIGURE 8.** Flow topology at both bleed ports near the endwall, RANS

lower left to upper right direction. Streamlines indicate the capturing streamtube of the bleed air flow. One can observe that the bleed flow at the VBP bleed port is quite straight and particularly the low momentum flow adjacent to the endwall is discharged. Despite a slight bleed amount which is spilled back into the passage (negative bleed) there is obviously no negative effect on the passage flow as it is shown by the straight wall friction lines at the blade and the endwall solids downstream of the bleed cavity. In contrast to that, the reference bleed port looks conspicuously inhomogeneous. This bleed geometry only partly removes the fluid from a developed separation region (lucent greenish isosurface) at the blade corner. Additionally, a larger amount of bleed air is spilled and again sucked by the cavity causing a displacement of the core flow which is suspected to be a cause of the flow separation at the blade itself. At the endwall downstream of the bleedport the surface streamlines indicate a newly formed disadvantageous longitudinal vortex rotating in the same direction like the secondary vortex.

The VBP principle which has been found to work well in the compressor cascade shall be illustrated more detailed in Fig. 9. The main flow comes from the left while the blade surface adjacent to the lower edge of the inlet is not shown. The velocity component into the cavity (spanwise velocity  $v_z$ ) in four planes perpendicular to the local streamwise direction is plotted. Blue lines represent velocity values into the cavity as they are aspired for a homogeneous removal. The lucent bluish isosurfaces indicate areas of axial backflow on the ramp and the sidewalls. The volume streamlines demonstrate the strong vortex generation and its trajectory which enables the port to homogeneously

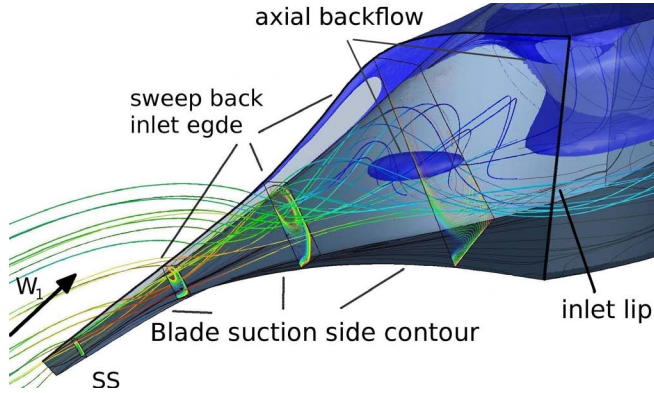


FIGURE 9. Flow topology within the VBP cavity, RANS

remove the bleed fluid from the main flowpath. Even though the vortex breaks down in the rear part of the section the flow stays attached to the ramp for a long distance which was an applicable indicator for the operating state of the port. This will be analyzed by means of pressure measurements later in the paper.

### Wake plane measurements

The five-hole probe measurements form the base of the experimental bleed port investigations. In Fig. 10 and 11 the two-dimensional distributions of the loss coefficient  $\zeta_V$  and the outlet angle  $\beta_2$  are illustrated. The cascade configuration without bleed (planar endwall) is placed at the top, the reference bleed port is placed in the middle and the results for the tailored VBP port can be found at the bottom. Likewise the numerical results are given at the right. For each sub-plot the half of the passage adjacent to the bleed side is shown. In the contour plots the blade suction side is above the profile wake and the endwall is at the left. The loss coefficient plot of the clean configuration shows the typical wake of a corner separation at the blade suction side with the corresponding pattern of over- and underturning in the deviation plot. This is satisfactorily predicted by the CFD where the intensity of secondary loss in the experiment is lightly increased. In low-speed cascades, the development of the corner separation is sensitive to endwall boundary layer properties as it was observed for related investigations, [14].

For the reference bleed configuration the total pressure loss could be decreased due to the partly extraction of fluid from the corner separation. Nevertheless, the local maximum of total pressure loss adjacent to the endwall is displaced towards the pressure side. The underturning at about 12 percent of the span has been damped but the overturning adjacent to the endwall is almost unchanged which is a result of the strong discharge near to the trailing edge. Near the endwall at  $y/t = -0.15$  a remarkable turning beyond the axial direction ( $\beta_2 < 0$ ) can be observed. However, this is found to be unfavorable as it decreases the pressure rise for the cascade and will be harmful for downstream

	Loss coefficient $\zeta_V / \zeta_{V, noBleed}$	Bleed pressure $\Delta p / q_{Bleed}$
No bleed	1.0	-
Reference port	0.49 (0.42)	-0.07 (-0.07)
VBP port	0.40 (0.43)	0.16 (0.122)

TABLE 1. Global flow performance ( $0 \leq z/h \leq 0.5$ ) for experiment and CFD (in parenthesis)

blade rows in the machine. This overturning is complementary to the vortex found in the wall streamlines in Fig. 8 (b).

The VBP bleed port leaves an improved wake pattern without the described negative effect in deviation as seen for the reference configuration above. The flow appears almost two dimensional near the endwall, hence demonstrating the success in suppressing the secondary flow. The numerical results confirm the positions of local maxima of losses with the restriction that the corner separation is persistently underpredicted. Note that the measurements start due to the diameter of the five-hole probe at a certain distance to the endwall ( $z = 5$  mm for reference and  $z = 2$  mm for the VBP port).

In Fig. 12 the pitchwise-averaged distributions for the loss coefficient  $\zeta_V$  and the outlet angle  $\beta_2$  are plotted. The curves for the loss coefficient confirm the observation from the planar distributions that the secondary losses were underpredicted by the CFD. Otherwise the measured profile losses for  $z/H \geq 0.3$  are reduced due to the laminar part of the blade surface in the experiment. While for the CFD data with bleed the vortex bleed port indicates reduced losses only near to the sidewall it is superior to the reference bleed port along the complete half-span in the experiment. The pitchwise distributions of the outlet angle  $\beta_2$  are plotted in the lower partfigure. At midspan the design outlet angle  $\beta_{2, Ref} = 18^\circ$  can be observed for the experimental data. For CFD it is increased by approximately one degree because of the fully turbulent approach. The devolution of the outlet angle with deflections due to over- and underturning is predicted satisfactorily. Both, numerical and experimental data show with a variation of  $\Delta\beta_2 \approx 2^\circ$  a quite homogeneous flow for the new vortex bleed port. Considering the loss coefficient and the outlet angle distribution of the reference bleed port the measured characteristics are remarkably decreased compared to the CFD prediction.

The relative variation of the integral values for the loss coefficient  $\zeta_V$  and the pressure recovery of the bleed air  $\Delta p / q_{Bleed}$  are summarized in Table 1. The experimental and the numerical loss coefficient values are given for the considered half passage with bleed disregarding the tip vortex influence at the hub. Generally, the characteristics of the core flow could be significantly improved by both bleed configurations. The total pressure loss was reduced by up to 60 percent for the VBP port which im-

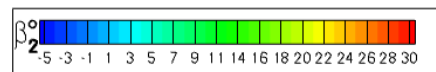
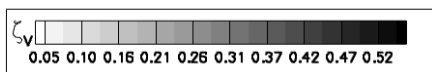
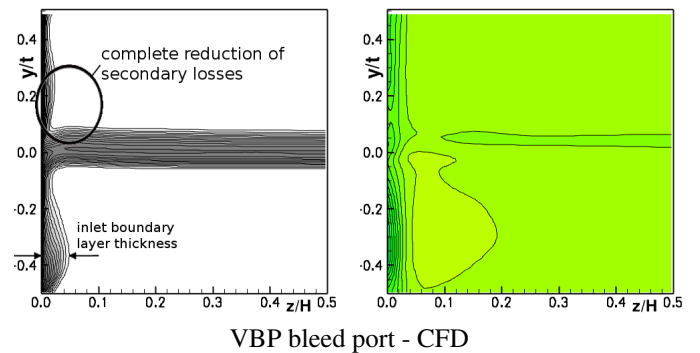
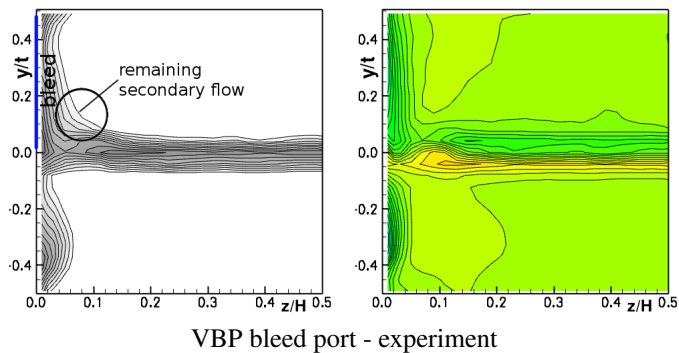
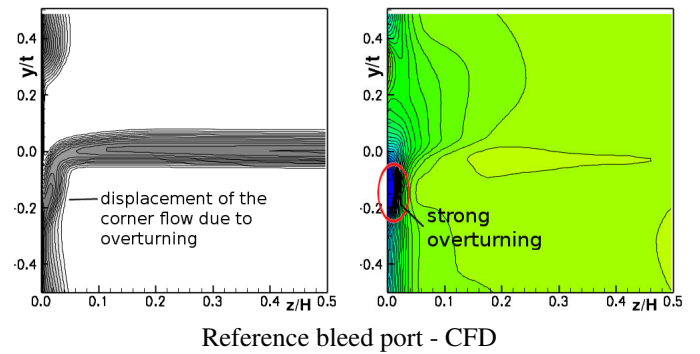
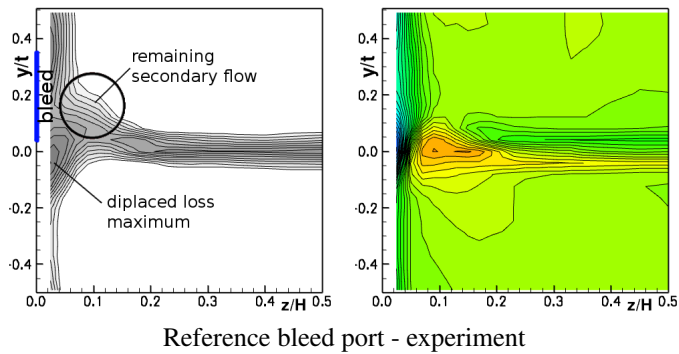
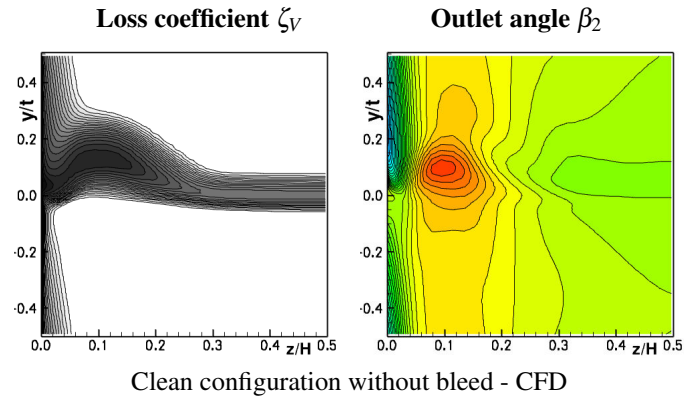
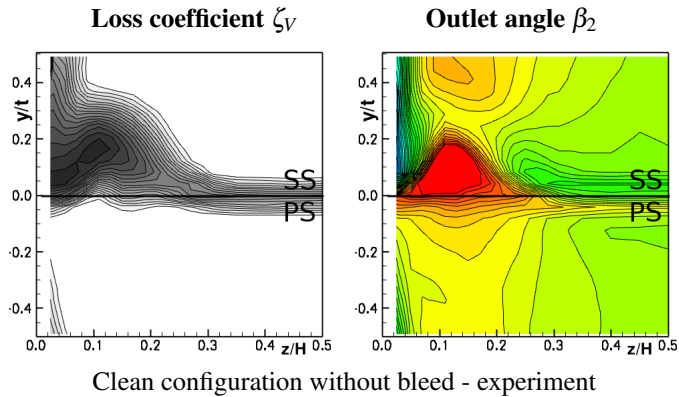


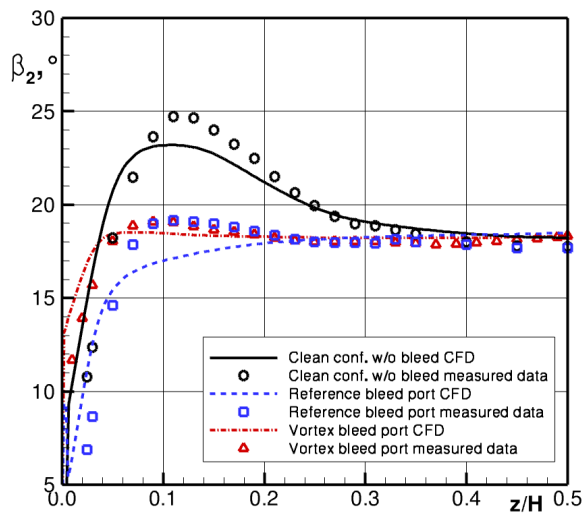
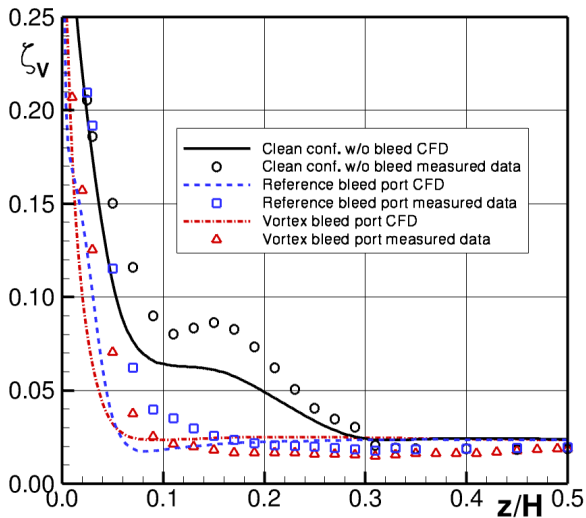
FIGURE 10. Flow in the wake plane - measurement

FIGURE 11. Flow in the wake plane - RANS

plies a complete suppression of the secondary flow. The pressure recovery of the bleed air is negative for the reference port, implying reduced pressure in the secondary system compared to the passage inlet. The VBP port recovers 16 percent of the inlet dynamic head. In comparison, the pressure recovery of an submerged NACA duct [11] for aircraft inlet purposes reaches up to 75 percent - but without having to deflect the removed flow by  $\Delta\alpha = 70^\circ$ .

### Oil flow visualizations

The wall-near flow phenomena for the configurations are presented with the help of oil flow pictures and wall shear stress lines for CFD. In figure 13 the full-span blade suction sides for the three configurations are shown. The laminar separation bubble at approximately 30% of chord length indicates the transition location for the wind tunnel experiment. Towards the endwall the laminar flow portion degenerates caused by the fully turbu-



**FIGURE 12.** Pitchwise-averaged results for loss coefficient  $\zeta_V$  and deviation angle  $\beta_2$

lent endwall boundary layer. Related investigations using transition strips in the experiment revealed that the separation bubble has no significant effect to the considered phenomena. The case without bleed offers the characteristic flow picture for a moderate corner separation of a low aspect ratio blade which affects about 25 percent of the span. This is essential for the loss characteristics of the investigated cascade.

The CFD calculations reflect the same flow topology with the constraint that the transitional effects are neglected. For the reference bleed port the corner flow region on the blade is decreased. A separation focal point has formed as it was predicted by the RANS simulations. Additionally, along a broad part of

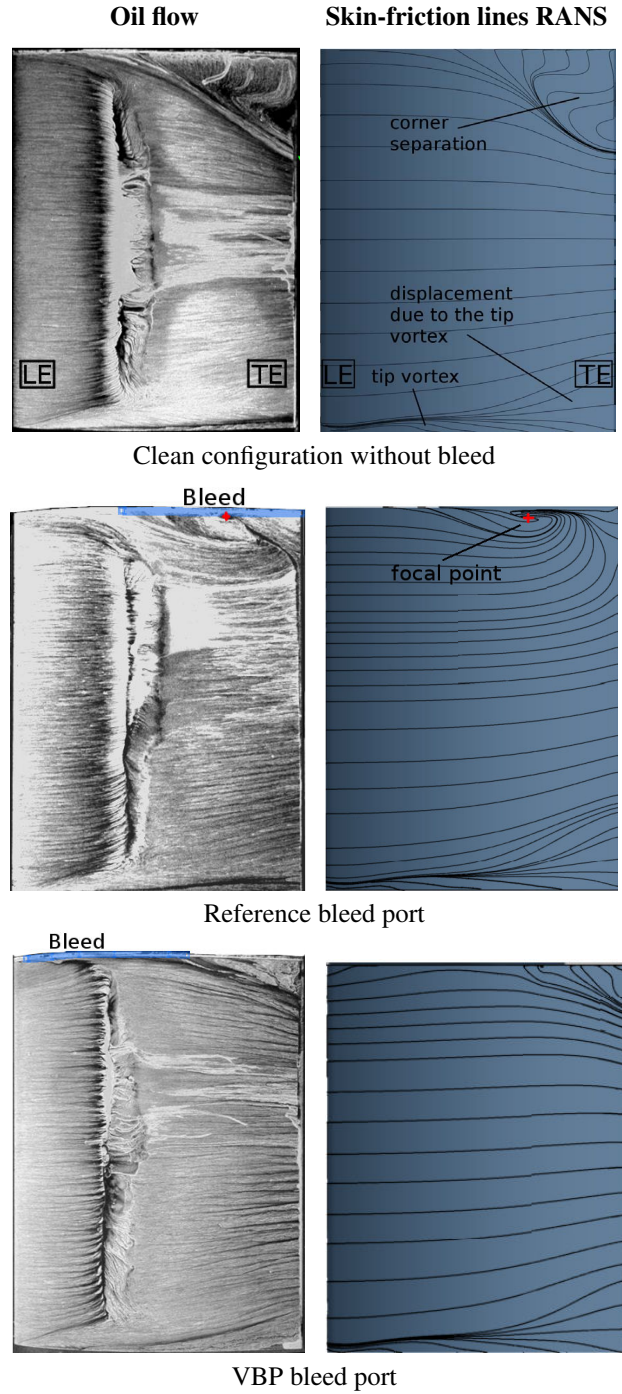


**FIGURE 13.** Flow visualizations of the blade suction side

the span the streamlines shift to the offtake side which indicates a strong redistribution within the passage. The flow at the VBP port shows clear advantages as the secondary flow on the blade is diminished to a very small corner with less cross-flow. At the opposite endwall the streamlines on the suction side are influenced

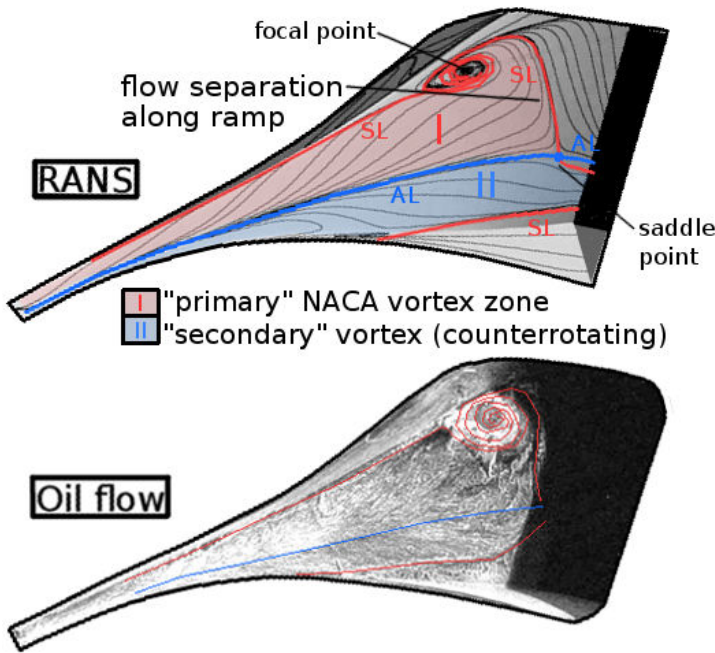


FIGURE 14. The wall-near flow topology within the VBP cavity

by the tip vortex indicating some remaining interaction between both endwalls if bleed removal is present.

In Fig. 14 the flow at the VBP port is illustrated by surface streamlines for the CFD data and an oil flow picture from the wind tunnel. At the wetted solids in the cavity a complex flow pattern of characteristic lines forms due to the three-dimensional flow. Earlier in the paper the strong longitudinal vortex was found to be important for the functionality of the duct as it charges fluid into the cavity. The footprint of this so-called primary NACA vortex is marked lucent red (I) in the upper part of the figure. The induced swirl of the vortex becomes apparent at the ramp surface in terms of streamlines which converge respectively diverge to a pair of separation (SL) and attachment lines (AL). After about 70% of the streamwise path along the ramp the flow separates at another separation line which merges in a focal point. The blue marked area (II) on the surface indicates the existence of a secondary counterrotating vortex. For well performing configurations this inferior vortex is located below the utile primary vortex (see isolines for spanwise velocity in Fig. 9) thus having no significant effect on the bleed offtake mechanism. Due to several circumstances like the oil flow properties, accessibility and illumination no better photography of the cavity which had to be taken during the wind tunnel run could be accomplished. While the spiral point is well visible in the oil flow picture, the correct devolution of all characteristic lines is not completely apparent. But the picture does confirm the development of the longitudinal vortex trajectory and its separation

from the ramp surface. As additional verification of the bleed port mechanism, further calculated surface streamline plots for selected CFD studies are discussed in the appendix.

### Surface pressure measurements

A further comparison of the numerical prediction and experiments of both bleed configurations is performed by using surface pressure data. In Fig. 15 the blade suction side pres-

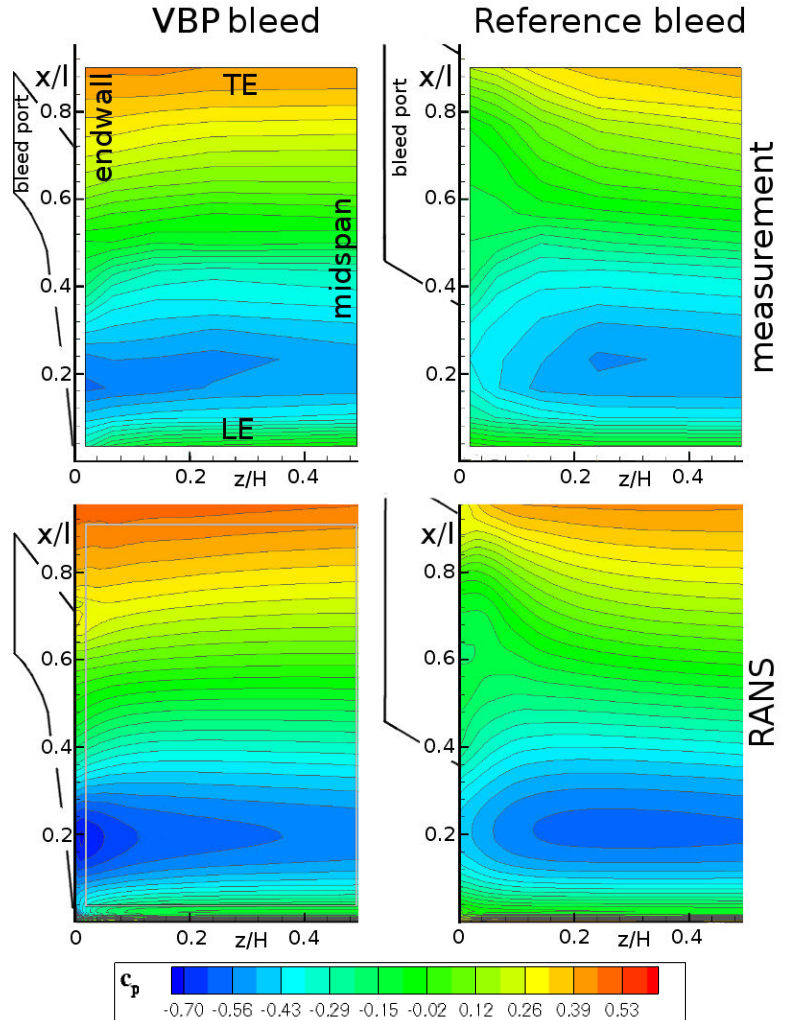


FIGURE 15. Surface pressure distribution at the blade suction side

sure distributions for the VBP (left column) and the reference bleed port (right column) are illustrated. Each sub-figure shows a half-span blade with the bleed cavity at the left side. The flow comes from below. The experimental plots are based on a data point mesh consisting of five spanwise arranged rows each with

15 chordwise pressure taps. Considering the left partfigures, one can observe that the early starting offtake causes a surface pressure distribution which has almost two dimensional properties. The suction peak near the cavity is amplified due to the additional velocity of the longitudinal vortex.

The reference bleed port shows an unlike inhomogeneous pattern in the pressure distribution. The gained pressure coefficients towards the trailing edge are slightly decreased. The bleed-offtake at the rear part of the blade shifts the load downstream. Considering the challenging wind tunnel boundary conditions, the experiments confirm all the observed effects, providing further confidence to the CFD results.

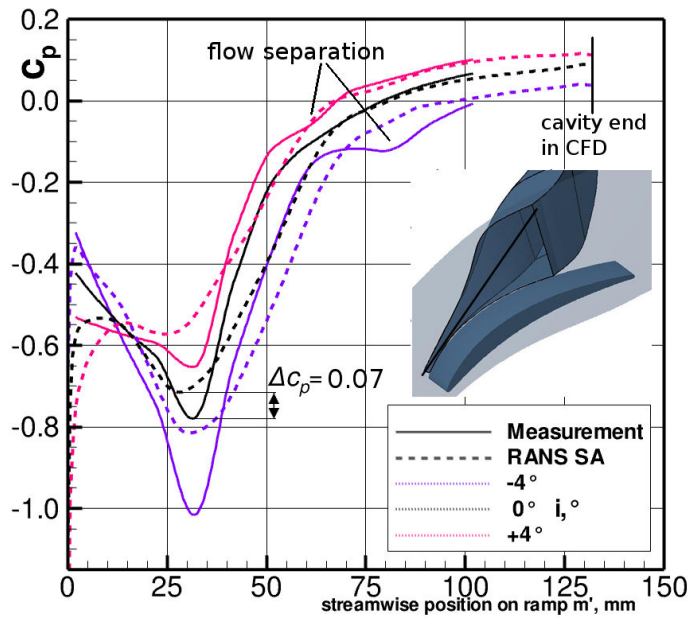


FIGURE 16. Pressure distribution along VBP ramp

In the next plot some of the results of the pressure tap measurements along the centerline of the ramp are presented. This complements the oil-flow pictures with quantitative data. In Fig. 16 the streamwise pressure distribution of the CFD results (dashed lines) and measured values (approximated by a solid spline curve) for design inlet angle  $\beta_1 = 48^\circ$  and off-design  $i_1 = \pm 4^\circ$  (color coding) is plotted. The data points start at approximately  $x/l = 2\%$  and end at the axial position of the inlet lip ( $x/l = 70\%$ ) with a deflection angle of  $\alpha = 40^\circ$ . The flow direction is hence from left to the right. Generally, the curves start with a drop in pressure down to a local minimum which results from the combination of the profile pressure distribution and the additional velocities caused by the vortex. Further along the ramp the pressure continuously levels off at the magnitude representative for the cavity outlet. On this way a local flow sep-

aration is indicated by a sectional discontinuity in the pressure coefficient. In the experiment the pressure minimum axial position stays fixed at  $m' = 32$  mm for different cascade inlet angles  $\beta_1$ . Based on the fact that the profile suction peak travels downstream for increased incidence the vortex intensity maximum apparently has been shifted downstream. This effect is unascertainable in the CFD curves where the generally increased pressure minimum is traveling upstream with increased incidence. As the blade pressure distribution for the experiment and RANS match very well (shown for design inlet angle in Fig. 15) the vortex intensity seems to be underpredicted by the CFD so that the suction peak of the blade pressure distribution is dominant. This decreased vortex intensity is common for linear eddy-viscosity turbulence models as they lead to exceeded damping of longitudinal vortices. Nevertheless, the separation position along the ramp is similarly predicted by RANS. Despite an increased separation intensity in the experiment, the achieved pressure recovery at the cavity outlet is in good agreement.

### Pressure recovery characteristics

In Table 1 the bleed air pressure recovery values for design inlet angle were already provided. Using Fig. 17, the offtake

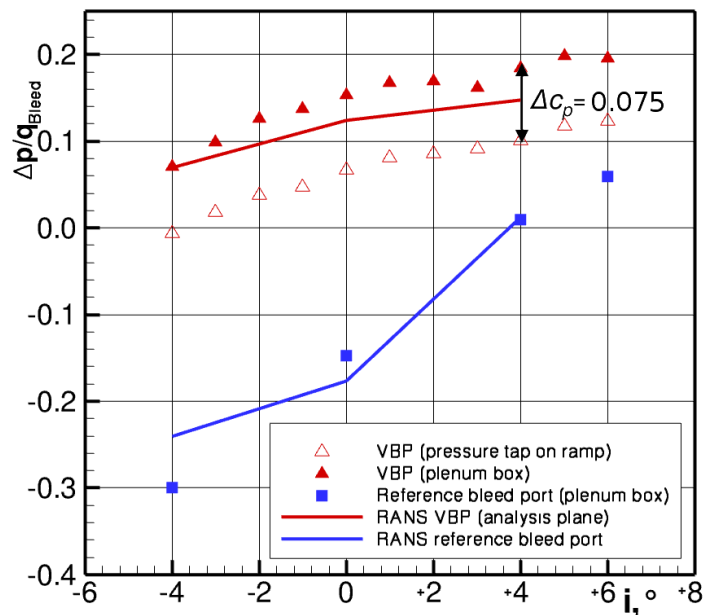


FIGURE 17. Pressure recovery for both bleed configurations for variable incidence

behavior is discussed more detailed. The pressure recovery coefficient  $\Delta p/q_{Bleed}$  is plotted over the cascade incidence  $i$ . The relative bleed massflow is kept constant at  $\dot{m}_{Bleed}/\dot{m}_1 = 3\%$  for every point. The filled symbols are measured pressures within

the plenum box. For both bleed configurations the pressure increases with throttling of the passage. The VBP port delivers throughout higher pressures. For the VBP configuration additional data was available by means of the last pressure tap in streamwise direction at the ramp which is shown by the hollow triangles. The offset between the triangles hence indicates a constant additional pressure recovery within the plenum box with  $\Delta c_{p,Bleed} \approx 0.075$ . Further the values predicted by CFD are printed as thick solid lines based on three simulated inlet angles. This calculated pressure coefficient represents a mass-averaged value at the bleed analysis plane and yields results somewhere between the pressure level at the ramp end and the plenum box. Both, the level and the trend of pressure recovery could be predicted well.

## CONCLUSIONS

In the paper a novel geometry for compressor secondary air offtake has been introduced. The bleed design enables a smooth discharge of endwall-near fluid hence reducing the cross flow vortex in a compressor passage. The formation of a strong longitudinal vortex within the cavity facilitates the fluid removal from critical regions and reduces leakage back into the passage. Consequently, the main flow could be further improved in terms of loss coefficient and pressure rise compared to an already well performing reference configuration. Despite the expected additional stagnation pressure loss due to the strong vortex formation the bleed pressure recovery could also be enhanced. For a fixed bleed rate of 3% the passage loss coefficient for the considered half of the passage was reduced by more than 50% in comparison to the configuration with planar endwall which implies a significant reduction of the secondary loss for the cascade.

The comparison between experimental and numerical results overall pointed out a good agreement even if the accuracy of some of the flow details and absolute values are in need of improvement. For the presented investigations, the numerical simulations using the Spalart-Allmaras turbulence model were found to be suited for design process dealing with the present complex vortex flow.

## ACKNOWLEDGMENT

The investigations were conducted as part of the joint research project 'VerDeMod' in the frame of the LUFO IV programme. The work was funded by Rolls-Royce Deutschland and the Bundesministerium für Wirtschaft und Technologie (BMWi) as per resolution of the German Federal Parliament under the Grant number 20T0609. The authors gratefully acknowledge Rolls-Royce Deutschland for their support and the permission to publish this paper.

## REFERENCES

- [1] Cumpsty, N.A. *Compressor Aerodynamics*, Krieger, Malabar Florida, 2004.
- [2] Bowman R. *Bleed Slot Efficiency*, PhD Thesis, Cambridge University, 1996.
- [3] Gomes R.A., Schwarz C., Pfitzner M. *Aerodynamic Investigations of a Compressor Bleed Air Configuration Typical for Aeroengines*, ISABE-2005-1264, Proceedings of XVII ISABE, Munich, 2005.
- [4] Schwarz C. *Aerodynamische Untersuchungen an Abblase-Luftsystemen mehrstufiger Axialverdichter*, PhD Thesis, Universität der Bundeswehr, München, 2005.
- [5] Willis B.P., Davis D.O., Hingst W.R. *Flow Coefficient Behavior for Boundary Layer Bleed Holes and Slots*, NASA Technical Memorandum No. 95-0031, Lewis Research Center, Ohio 1995.
- [6] Leishman B.A., Cumpsty N.A., Denton J.D. *Effects of Bleed Rate and Endwall Location on the Aerodynamic Behavior of a Circular Hole Bleed Off-Take*, Journal of Turbomachinery, Vol. 129, pp. 645-658, 2007.
- [7] Leishman B.A., Cumpsty N.A., Denton J.D. *Effects of Inlet Ramp Surfaces on the Aerodynamic Behavior of Bleed Hole and Bleed Slot Off-Take Configurations*, Journal of Turbomachinery, Vol. 129, pp. 659-668, 2007.
- [8] Leishman B.A., Cumpsty N.A. *Mechanism of the Interaction of a Ramped Bleed Slot with the Primary Flow*, Journal of Turbomachinery, Vol. 129, pp. 669-678, 2007.
- [9] Gümmer V., Goller M., Swoboda M. *Numerical Investigations of Endwall Boundary Layer Removal on Highly-Loaded Axial Compressor Blade Rows*, GT2005-68699, Proceedings of ASME Turbo Expo, Reno-Tahoe, 2005.
- [10] Conan F., Savarese S. *Bleed Airflow CFD Modeling in Aerodynamics Simulation of Jet Engine Compressors*, 2001-GT-544, Proceedings of ASME Turbo Expo 2001, New Orleans, 2001.
- [11] Frick C.W., Davis W.F., Randall L.M., Mossman E.A. *An Experimental Investigation of NACA Submerged Duct Entrances*, NACA ACR 5I20, Ames Aeronautical Laboratory, Washington, 1945.
- [12] NUMECA Users Manual *Flow Integrated Environment<sup>TM</sup>/Turbo v8.3-1*, Brussels, Belgium, 2009.
- [13] Nerger D. *Aktive Strömungsbeeinflussung in ebenen Statorgittern hoher aerodynamischer Belastung durch Ausblasen*, PhD Thesis, Technische Universität Braunschweig, 2009.
- [14] Pönick S., Kožulović D., Radespiel R., Becker B., Gümmer V. *Numerical and experimental studies of the flow field details on a cascade with endwall part-clearance* ETC2009, Graz, Austria, 2009.

## Appendix Numerical sensitivities

In the following chapter some results of numerical sensitivity investigations are discussed. In Fig. 18 the wall streamlines on the VBP ramp surface comparable to Fig.14 are shown. The

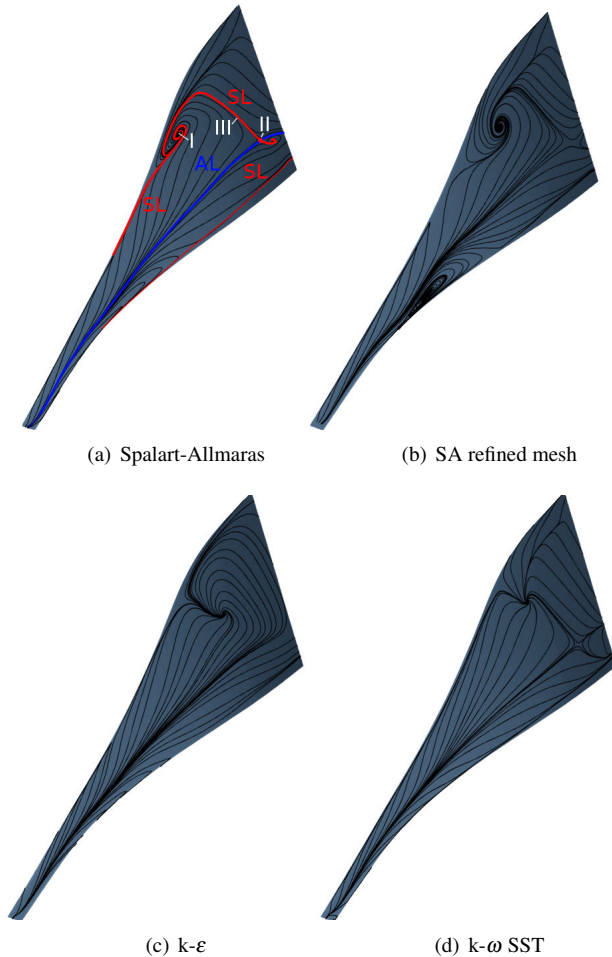


**FIGURE 18.** Surface streamlines on VBP ramp for different turbulence models

partfigures (a) and (b) show the results for the Spalart-Allmaras turbulence model for the reference mesh (a) and a globally<sup>1</sup> refined mesh (b) with halved cell width (21 million cells). In the partfigures (c) and (d) the streamlines for the  $k-\varepsilon$  by Chien and  $k-\omega$  SST turbulence model are plotted. In the first two partfigures one can observe only little changes in the devolution of the characteristic lines and the forming of the focal (I) and saddle (II) point. Important for the cavity flow and hence the pressure recovery is the separation line transverse to the main flow direction

<sup>1</sup>only the half of the passage adjacent to the bleed port was refined due to CPU and memory reasons

(III). Compared to the reference simulation (a) this separation is shifted downstream for the refined mesh (b) and displaced upstream for the SST turbulence model (d). The  $k-\varepsilon$  simulation (c) shows the most extensive topology change as the primary vortex zone is interrupted by a broader focal point. Furthermore the separation line (III) and the saddle point (II) are not existing.

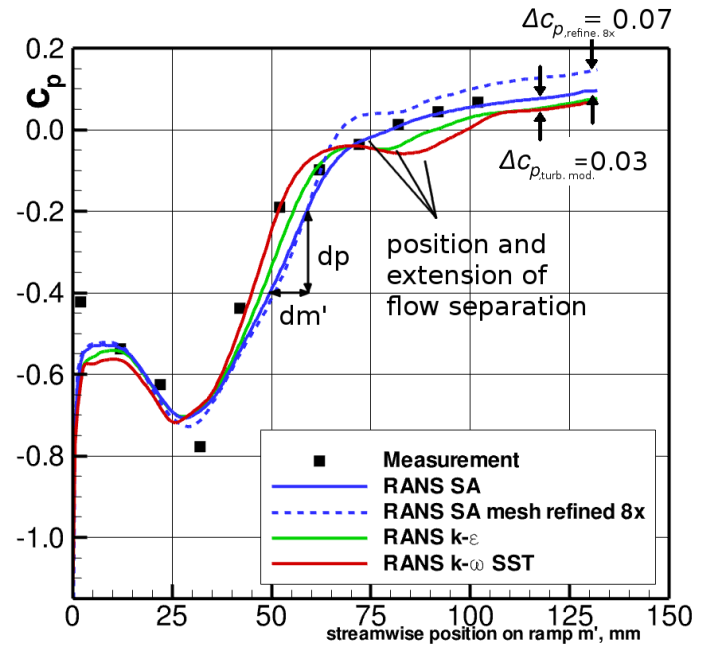


**FIGURE 19.** Sensitivities of pressure distribution along VBP ramp

The numerical sensitivities of the pressure distribution are plotted in Fig. 19. For the different turbulence models within the first  $m' = 30$  mm only slight variations of the pressure coefficient and hence velocity distribution occur. The minimum pressure which represents the vortex peak velocities are almost equal in position and value within  $\Delta c_p \approx 0.015$ . Only the refined mesh shows clearly decreased pressure minimum and hence tends to the measured data. As the wall streamline plots in Fig. 18 indicated a different separation behavior the pressure distributions in the rear part of the ramp show consistent variations. The two-equation turbulence models predict an earlier starting and stronger decay of the longitudinal vortex in terms of an increased adverse pressure gradient  $dp/dm' > 0$  in combination with a larger flow separation (see focal point for  $k-\varepsilon$ ). This results in a decreased pressure recovery at the end of the ramp. The Spalart-Allmaras simulation on the refined mesh shows an increased pressure recovery of  $\Delta c_p = 0.07$  as it has been mentioned earlier in the paper. Considering the highly three-dimensional cavity flow and limitations of the applied linear eddy-viscosity models, the agreement of the predicted pressure distributions is good.

Finally the sensitivity of flow topology within the passage for both offtake configurations is discussed. In Fig. 20 the corner flow between bleed port and trailing edge is visualized in terms of surface streamlines. Further the spanwise velocity  $v_z$  through the bleed inlet area is plotted. At the vortex bleed port (partfigures a-d) the flow at the endwall is subjected to only small changes within topology near the trailing edge in terms of position and development of a reattachment nodal point (b+c) or reattachment focus (a+d). For the reference mesh with Spalart-Allmaras turbulence model only one separation line can be observed in the out-flow direction. The flow separation at the endwall downstream of the area with negative bleed (red contour values  $v_z > 0$ ) is decreased for the SST simulation only. The two-equation turbulence models indicate a further decrease of the corner separation on the blade which was already found to be underpredicted by the Spalart-Allmaras turbulence model in comparison to the measurement. Nevertheless, the wall-near flow is very similar for all simulations.

For the reference bleed configuration (partfigures e-h) turbulence model and mesh refinement show slightly increased influence. The extension and strength of the focal point on the blade suction side slightly differs between the cases. At the endwall downstream of the trailing edge the unfavorable longitudinal vortex is a little sensitive to the numerical parameters. The detailed topology of the wall streamlines depends on the CFD setup similarly to the VBP configuration. For the refined mesh (f) the trailing edge vortex becomes apparent in terms of an additional attachment and separation line. The sub-figures (i)+(j) show the accordant oil flow pictures for the wind tunnel experiment. The three characteristic lines described above for the CFD results can be found in the oil flow visualizations, too.

In summary, the largest sensitivity for both bleed configurations is given for the SST simulations what was confirmed by the ramp pressure distribution and the passage flow pictures. The simulation with strongly refined mesh in combination with Spalart-Allmaras shows a further improvement toward the measurement. Nevertheless, a general conclusion which turbulence model is the most appropriate one for the present flow could not be made. Altogether, the apparently moderate sensitivity of the vortex within the cavity, the consistent pressure data on the ramp and especially the low effect on the remaining secondary flow in the passage are providing further confidence to the CFD results. The reference mesh resolution (5.2 million cells) which should be near the actual limit for a multi-row simulation is found to be sufficient.

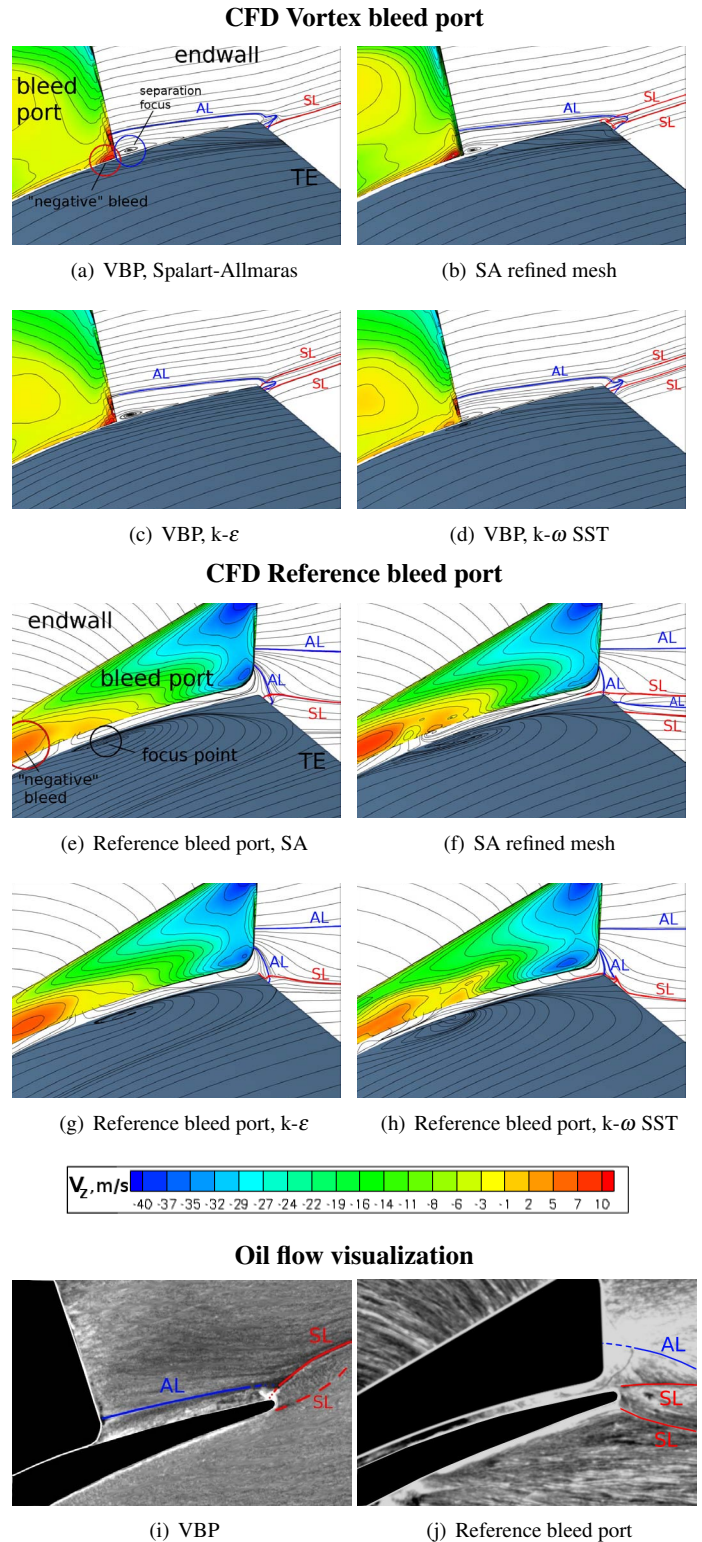


**FIGURE 20.** Surface streamlines and radial velocity distribution for both bleed configurations for different turbulence models